

# Universal quantum gates for hybrid systems assisted by quantum dots inside double-sided optical microcavities\*

Hai-Rui Wei and Fu-Guo Deng<sup>†</sup>

*Department of Physics, Applied Optics Beijing Area Major Laboratory,  
Beijing Normal University, Beijing 100875, China*

(Dated: October 14, 2018)

We present some deterministic schemes to construct universal quantum gates, that is, controlled-NOT, three-qubit Toffoli, and Fredkin gates, between flying photon qubits and stationary electron-spin qubits assisted by quantum dots inside double-sided optical microcavities. The control qubit of our gates is encoded on the polarization of the moving single photon and the target qubits are encoded on the confined electron spins in quantum dots inside optical microcavities. Our schemes for these universal quantum gates on a hybrid system have some advantages. First, all the gates are accomplished with a success probability of 100% in principle. Second, our schemes require no additional qubits. Third, the control qubits of the gates are easily manipulated and the target qubits are perfect for storage and processing. Fourth, the gates do not require that the transmission for the uncoupled cavity is balanceable with the reflectance for the coupled cavity, in order to get a high fidelity. Fifth, the devices for the three universal gates work in both the weak coupling and the strong coupling regimes, and they are feasible in experiment.

PACS numbers: 03.67.Lx, 42.50.Ex, 42.50.Pq, 78.67.Hc

## I. INTRODUCTION

Quantum logic gates lie at the heart of quantum information processing. Two-qubit controlled-not (CNOT) gates together with single-qubit gates are sufficient for universal quantum computing [1, 2]. The optimal synthesis and the “small-circuit” structure for two-qubit systems have been well solved [3–6], while the case for multi-qubit systems is quite complex. Up to now, it has also been an open question. That is, it is significant to seek a simpler scheme for directly implementing multi-qubit gates. In the domain of three-qubit gates, Toffoli and Fredkin gates have attracted much attention and both these two gates are universal. Together with Hadamard gates, they form a universal quantum computation architecture [7, 8]. Moreover, they play an important role in phase estimation [1], complex quantum algorithms [9], error correction [10], and fault tolerant quantum circuits [11].

Quantum logic gates between flying photon qubits and stationary (matter) qubits hold great promise for quantum communication and computing since photons are the perfect candidates for fast and reliable long-distance communication because of their robustness against decoherence, while the stationary qubits are suitable for processor and local storage. In 2005, Liang and Li [12] chose atoms or ions as the matter qubit to discuss the realization of a two-qubit SWAP gate. One of the attractive candidates for a stationary qubit is the electron spin in a GaAs-based or InAs-based charged quantum dot (QD). The electron-spin coherence time of a charged QD [13–18]

can be maintained for more than 3  $\mu$ s [19, 20] using spin echo techniques, and the electron spin-relaxation time can be longer ( $\sim$  ms) [21, 22]. Moreover, it is comparatively easy to incorporate a QD into a solid-state cavity, and fast QD-spin cooling and manipulation have had some significant progress [23–26]. These results indicate that the excess electron spin confined in a QD can be used for a stable and scalable quantum computation. Based on a singly charged QD inside an optical resonant cavity [27, 28], in 2010 Bonato *et al.* [29] proposed a theoretical scheme for a CNOT gate with the confined electron spin as the control qubit and the polarization photon as the target qubit. This QD-cavity system has been used for a two-photon Bell-state analyzer, entanglement generators, teleportation, entanglement swapping, quantum repeaters, entanglement purification and concentration, and hyperentangled-Bell-state analysis [27–35].

Different from the work by Bonato *et al.* [29] in which they presented a scheme for a CNOT gate with a confined electron spin in a QD as the control qubit and a flying photon as the target qubit, we first present a deterministic scheme for constructing a CNOT gate on a hybrid system with the flying photon as the control qubit and the excess electron in a QD as the target qubit. Also, we propose two deterministic schemes for constructing the Toffoli and Fredkin gates on a three-qubit hybrid system. In our work, the control qubits of our universal gates are encoded on the moving photon qubit (i.e., the two polarization states of a single photon, denoted by  $|R\rangle$  and  $|L\rangle$ ), while the target qubit is encoded on the spin of the excess electron confined in a QD inside an optical microcavity (denoted by  $|\uparrow\rangle$  and  $|\downarrow\rangle$ ). These three schemes for the universal gates require no additional qubits, and they only need some linear optical elements besides the nonlinear interaction between the moving photon and the electron in a QD inside an optical microcavity. It is worth

\*Published in Phys. Rev. A **87**, 022305 (2013)

<sup>†</sup>Corresponding author: fgdeng@bnu.edu.cn

pointing out that these gates are robust because they do not require that the transmission for the uncoupled cavity is balanceable with the reflectance for the coupled cavity in order to get a high fidelity, different from the hybrid gates which are encoded on the spin confined in a QD inside a single-sided cavity [28]. The fidelities and the efficiencies of our gates are discussed. A high fidelity and a high efficiency can be achieved in both the strong and the weak regimes, and our devices are feasible with current experimental technology.

This paper is organized as follows: In Sec.II, we briefly review a singly charged QD in a double-sided optical microcavity. In Sec.III, we propose a deterministic scheme for constructing a two-qubit CNOT gate between a flying photon (the control qubit) and a stationary electron (the target qubit) confined in a QD. The fundamental three-qubit gates, Toffoli (control-CNOT) and Fredkin (control-SWAP) gates, on a three-qubit hybrid system are constructed in Secs.IV and V, respectively. The fidelity, the efficiency, and the experimental feasibility of our schemes for hybrid quantum gates are discussed in Sec.VI. Some discussions and a summary are given in Sec.VII.

## II. A SINGLY CHARGED QD IN A DOUBLE-SIDED MICROCAVITY

In 2009, Hu *et al.* [28] proposed a double-side QD-cavity system, which can be used for quantum computation, quantum communication, and quantum storage. In this appealing system, a singly charged electron In(Ga)As QD or a GaAs interface QD is embedded in an optical resonant double-sided microcavity with two mirrors partially reflective in the top and the bottom. The excess electron-spin qubit in the QD promises scalable quantum computation in solid-state systems, and it interacts with the cavity mode through the addition of a negatively charged exciton ( $X^-$ ) that consists of two electrons and one hole [36] created by excitation. The exciton determines the rules of the spin-dependent optical transitions (depicted in Fig.1) [37]. In this work, we consider the dipole resonance with the cavity mode and the input photon. The rules of the input states changing under the interaction of the photon and the cavity can be described as follows:

$$\begin{aligned} |R^\uparrow \uparrow\rangle &\rightarrow |L^\downarrow \uparrow\rangle, & |L^\uparrow \uparrow\rangle &\rightarrow -|L^\uparrow \uparrow\rangle, \\ |R^\downarrow \uparrow\rangle &\rightarrow -|R^\downarrow \uparrow\rangle, & |L^\downarrow \uparrow\rangle &\rightarrow |R^\uparrow \uparrow\rangle, \\ |R^\uparrow \downarrow\rangle &\rightarrow -|R^\uparrow \downarrow\rangle, & |L^\uparrow \downarrow\rangle &\rightarrow |R^\downarrow \downarrow\rangle, \\ |R^\downarrow \downarrow\rangle &\rightarrow |L^\uparrow \downarrow\rangle, & |L^\downarrow \downarrow\rangle &\rightarrow -|L^\downarrow \downarrow\rangle. \end{aligned} \quad (1)$$

There are two kinds of optical transitions between the electron and the exciton  $X^-$ , one involving the photon with the spin  $s_z = +1$  and the other involving the photon with the spin  $s_z = -1$ . For a photon with  $s_z = +1$  ( $|R^\uparrow\rangle$  or  $|L^\downarrow\rangle$ ), if the excess electron is in the spin state  $|\uparrow\rangle$ , it couples to the dipole and will be reflected by the cavity,

and both the polarization and the propagation direction of the photon will be flipped. If the excess electron spin is in the state  $|\downarrow\rangle$ , the photon in the polarization state  $|R^\uparrow\rangle$  or  $|L^\downarrow\rangle$  will not couple to the dipole, and it will transmit the cavity and acquire a  $\pi \bmod 2\pi$  phase shift relative to a reflected photon. In the same way, for the photon in the state  $|R^\downarrow\rangle$  or  $|L^\uparrow\rangle$  ( $s_z = -1$ ), if the excess electron spin is in the state  $|\uparrow\rangle$ , it will transmit the cavity. If the excess electron spin is in the state  $|\downarrow\rangle$ , it will be reflected by the cavity. That is, this structure ( $X^-$ -cavity system) acts as an entanglement beam splitter. It splits an initial product state of the system composed of an injecting photon and an electron spin into two entangled states via the transmission and the reflection of the photon in a deterministic way. Compared with a single-sided QD-cavity system, the doubled-sided unit easily reaches a large phase difference ( $\pi$ ) between the uncoupled cavity and the coupled cavity [28]. The device based on double-sided units is robust [28]. In the following, we investigate the construction of the universal hybrid quantum gates, that is, CNOT, Toffoli, and Fredkin gates, which take electron-spin qubits confined in QDs as the target qubits and a flying photon as the control qubit.

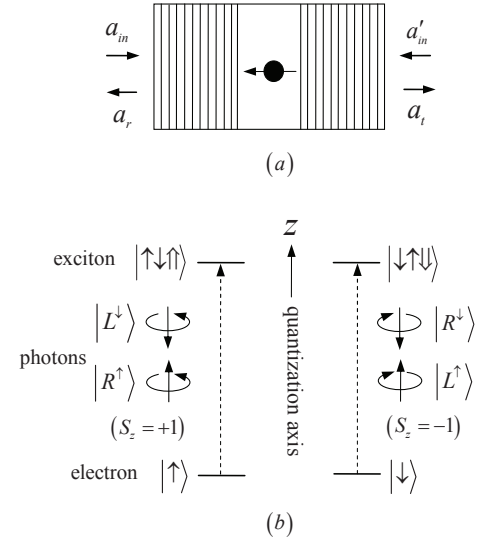


FIG. 1: (a) A schematic diagram for a singly charged QD inside a double-sided optical microcavity. (b) Schematic description of the relevant exciton energy levels and the spin selection rules for optical transition of negatively charged exciton. The symbols  $\uparrow$  ( $\downarrow$ ) and  $\uparrow$  ( $\downarrow$ ) represent a hole and an excess electron with  $z$ -direction spin projections  $|+\frac{3}{2}\rangle$  ( $|-\frac{3}{2}\rangle$ ) and  $|+\frac{1}{2}\rangle$  ( $|-\frac{1}{2}\rangle$ ), respectively.  $|R^\uparrow\rangle$  ( $|R^\downarrow\rangle$ ) denotes a right-circularly polarized photon propagating along (against) the normal direction of the cavity  $z$  axis (the quantization axis) and  $|L^\uparrow\rangle$  ( $|L^\downarrow\rangle$ ) denotes a left-circularly polarized photon propagating along (against) the  $z$  axis.

### III. CNOT GATE ON A TWO-QUBIT HYBRID SYSTEM WITH A FLYING PHOTON AS THE CONTROL QUBIT

The principle for a CNOT gate, which flips the target electron-spin qubit if the control photon polarization qubit is in the state  $|L\rangle$ , is depicted in Fig.2. The flying photon  $p$  and the excess electron  $e$  in a QD are prepared in arbitrary superposition states  $|\psi\rangle_p = \alpha_c|R\rangle + \beta_c|L\rangle$  and  $|\psi\rangle_e = \alpha_t|\uparrow\rangle + \beta_t|\downarrow\rangle$  (here  $|\alpha_c|^2 + |\beta_c|^2 = |\alpha_t|^2 + |\beta_t|^2 = 1$ ), respectively. The subscripts  $p$  and  $e$  represent the photon and the electron, respectively. The CNOT gate can be constructed with the steps shown in Fig.2.

First, the injecting photon passes through PBS<sub>1</sub> which transmits the photon in the polarization state  $|R\rangle$  and reflects the photon in the state  $|L\rangle$ . That is, PBS<sub>1</sub> splits the photon into two wave-packets. The part in the state  $|L\rangle$  is injected into the cavity and interacts with the QD, while the part in the state  $|R\rangle$  transmits PBS<sub>1</sub> and does not interact with the cavity. After the control photon passes through PBS<sub>1</sub>, the state of the whole system composed of a photon and an electron is changed from  $|\Psi_0\rangle$  to  $|\Psi_1\rangle$ . Here

$$\begin{aligned} |\Psi_0\rangle &= |\psi\rangle_p \otimes |\psi\rangle_e \\ &= (\alpha_c|R\rangle + \beta_c|L\rangle) \otimes (\alpha_t|\uparrow\rangle + \beta_t|\downarrow\rangle), \end{aligned} \quad (2)$$

$$\begin{aligned} |\Psi_1\rangle &= \alpha_c\alpha_t|R\rangle|\uparrow\rangle + \alpha_c\beta_t|R\rangle|\downarrow\rangle \\ &+ \beta_c\alpha_t|L\rangle|\uparrow\rangle + \beta_c\beta_t|L\rangle|\downarrow\rangle. \end{aligned} \quad (3)$$

Before the photon coming from the spatial mode 2 passes through PBS<sub>2</sub>, a Hadamard ( $H_p$ ) operation is performed on it with a half-wave plate (HWP) which is used to complete the transformations

$$|R\rangle \rightarrow \frac{1}{\sqrt{2}}(|R\rangle + |L\rangle), \quad |L\rangle \rightarrow \frac{1}{\sqrt{2}}(|R\rangle - |L\rangle), \quad (4)$$

and a Hadamard ( $H_e$ ) operation (e.g., using a  $\pi/2$  microwave pulse or optical pulse [25, 26]) is also performed on the electron to complete the transformations

$$\begin{aligned} |\uparrow\rangle &\rightarrow |\rightarrow\rangle \equiv \frac{1}{\sqrt{2}}(|\uparrow\rangle + |\downarrow\rangle), \\ |\downarrow\rangle &\rightarrow |\leftarrow\rangle \equiv \frac{1}{\sqrt{2}}(|\uparrow\rangle - |\downarrow\rangle). \end{aligned} \quad (5)$$

PBS<sub>2</sub> will lead the photon to paths 3 and 4 when the photon is in the states  $|R\rangle$  and  $|L\rangle$ , respectively. When the photon passes through path 4, it takes a phase shift  $\pi$  (i.e.,  $|L\rangle \rightarrow -|L\rangle$  and  $|R\rangle \rightarrow -|R\rangle$  when the photon passes through the device  $P_\pi$ ). That is, before the photon interacts with the QD inside the optical microcavity, the state of the photon-electron system becomes

$$\begin{aligned} |\Psi_2\rangle &= \alpha_c|R\rangle(\alpha_t|\rightarrow\rangle + \beta_t|\leftarrow\rangle) \\ &+ \frac{1}{2}\beta_c\alpha_t(|R\rangle + |L\rangle)(|\uparrow\rangle + |\downarrow\rangle) \\ &+ \frac{1}{2}\beta_c\beta_t(|R\rangle + |L\rangle)(|\uparrow\rangle - |\downarrow\rangle). \end{aligned} \quad (6)$$

The nonlinear interaction between the photon and the electron in the QD assisted by the optical microcavity makes the state of the system be changed as

$$\begin{aligned} |\Psi_3\rangle &= \alpha_c|R\rangle(\alpha_t|\rightarrow\rangle + \beta_t|\leftarrow\rangle) \\ &+ \frac{1}{2}\beta_c\alpha_t(-|R\rangle - |L\rangle)(|\uparrow\rangle - |\downarrow\rangle) \\ &+ \frac{1}{2}\beta_c\beta_t(-|R\rangle - |L\rangle)(|\uparrow\rangle + |\downarrow\rangle). \end{aligned} \quad (7)$$

When the photon  $p$  is in the state  $|R\rangle$ , it passes through the phase shifter  $P_\pi$  and reaches PBS<sub>2</sub> from path 4. When the photon  $p$  is in the state  $|L\rangle$ , it does not take a phase shift and reaches PBS<sub>2</sub> from path 3. Whether the photon passes through the path 4 or path 3, it is emitted from path 5 after an  $H_p$  operation is performed on it. Also, an  $H_e$  operation is performed on the electron spin. After the photon passes through PBS<sub>3</sub>, the state of the system becomes

$$\begin{aligned} |\Psi_4\rangle &= \alpha_c|R\rangle(\alpha_t|\uparrow\rangle + \beta_t|\downarrow\rangle) \\ &+ \beta_c|L\rangle(\alpha_t|\downarrow\rangle + \beta_t|\uparrow\rangle). \end{aligned} \quad (8)$$

From Eq.(8), one can see that the state of the electron (the target qubit) is flipped when the photon (the control qubit) is in the state  $|L\rangle$ , while it does not change when the photon is in the state  $|R\rangle$ , compared to the original state of the two-qubit hybrid system shown in Eq.(2). That is, the quantum circuit shown in Fig.2 can be used to construct a deterministic CNOT gate with a success probability of 100% in principle, by using the photon as the control qubit and the electron spin as the target qubit.

### IV. TOFFOLI GATE ON A THREE-QUBIT HYBRID SYSTEM

A three-qubit Toffoli gate is used to perform a NOT operation on a target qubit or not, depending on the states of the two control qubits [8]. In the optimal scheme for decomposing a three-qubit gate, it requires at least six CNOT gates for implementing a Toffoli gate [38], which increases the difficulty of its implementation by using the fundamental two-qubit gates and one-qubit gates. Therefore, it is desirable to seek a simpler scheme for directly implementing the three-qubit Toffoli gate.

Our device for implementing a deterministic Toffoli gate on a photon qubit and two electron-spin qubits is shown in Fig.3. When the control photon qubit (the flying photon) and the control electron-spin qubit (the electron in cavity 1) are in the states  $|L\rangle$  and  $|\downarrow\rangle$ , respectively, the state of the target electron-spin qubit (the electron in cavity 2) is flipped; otherwise, the state of the target electron-spin qubit does not change. We describe this principle in detail as follows.

Suppose that the flying photon qubit is prepared in an arbitrary superposition state

$$|\psi\rangle_p = \alpha_p|R\rangle + \beta_p|L\rangle, \quad (9)$$

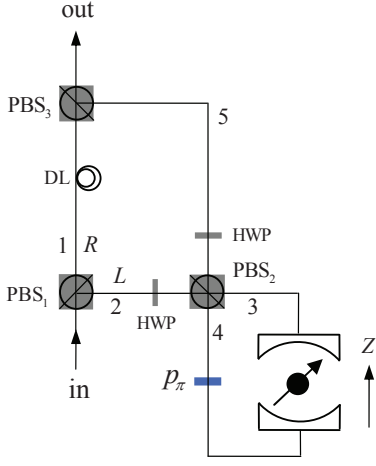


FIG. 2: (Color online) The quantum circuit for constructing a deterministic CNOT gate with a flying photon polarization as the control qubit and a confined electron spin as the target qubit.  $PBS_i$  ( $i = 1, 2, 3$ ) is a polarizing beam splitter in the circular basis, which transmits the right-circular polarization photon  $|R\rangle$  and reflects the left-circular polarization photon  $|L\rangle$ , respectively. HWP represents a half-wave plate which is set to  $22.5^\circ$  to induce the Hadamard transformations on the polarizations of photons.  $P_\pi$  is a phase shifter that contributes a  $\pi$  phase shift to the photon passing through it. DL is the time-delay device for making the photons from modes 1 and 5 reach  $PBS_3$  simultaneously. Before and after the photon interacts with the electron spin in the QD inside the double-side optical microcavity, a Hadamard ( $H_e$ ) operation is performed on the electron spin by using a  $\pi/2$  microwave pulse or an optical pulse.

and each of two independent excess electrons in cavities 1 and 2 is prepared in an arbitrary state as

$$\begin{aligned} |\psi\rangle_{e_1} &= \alpha_{e_1} |\uparrow\rangle_1 + \beta_{e_1} |\downarrow\rangle_1, \\ |\psi\rangle_{e_2} &= \alpha_{e_2} |\uparrow\rangle_2 + \beta_{e_2} |\downarrow\rangle_2. \end{aligned} \quad (10)$$

Here the subscript 1 (2) represents the electron in cavity 1 (2) and

$$|\alpha_p|^2 + |\beta_p|^2 = |\alpha_{e_1}|^2 + |\beta_{e_1}|^2 = |\alpha_{e_2}|^2 + |\beta_{e_2}|^2 = 1. \quad (11)$$

We first inject the flying photon  $p$  from  $PBS_1$  which splits the photon into two wave-packets, the part in the state  $|R\rangle$  and that in  $|L\rangle$ . When the photon is in the state  $|L\rangle$ , it passes through  $PBS_2$  and is injected into cavity 1. When the photon is in the state  $|R\rangle$ , it transmits  $PBS_1$  and does not interact with the cavity. After the photon passes through  $PBS_1$ , the state of the whole system composed of a flying photon and two stationary electrons is changed from  $|\Phi_0\rangle$  to  $|\Phi_1\rangle$ . Here

$$\begin{aligned} |\Phi_0\rangle &= |\psi\rangle_p \otimes |\psi\rangle_{e_1} \otimes |\psi\rangle_{e_2} \\ &= \alpha_p \alpha_{e_1} |R\rangle |\uparrow\rangle_1 (\alpha_{e_2} |\uparrow\rangle + \beta_{e_2} |\downarrow\rangle)_2 \\ &\quad + \alpha_p \beta_{e_1} |R\rangle |\downarrow\rangle_1 (\alpha_{e_2} |\uparrow\rangle + \beta_{e_2} |\downarrow\rangle)_2 \\ &\quad + \beta_p \alpha_{e_1} |L\rangle |\uparrow\rangle_1 (\alpha_{e_2} |\uparrow\rangle + \beta_{e_2} |\downarrow\rangle)_2 \end{aligned}$$

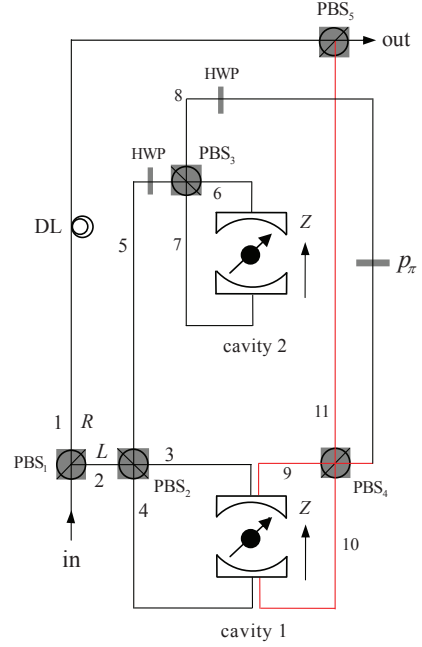


FIG. 3: (Color online) Scheme for implementing a three-qubit Toffoli gate with a flying photon polarization and a confined electron-spin qubit as the two control qubits and another confined electron-spin qubit as the target qubit.

$$+ \beta_p \beta_{e_1} |L\rangle |\downarrow\rangle_1 (\alpha_{e_2} |\uparrow\rangle + \beta_{e_2} |\downarrow\rangle)_2, \quad (12)$$

$$\begin{aligned} |\Phi_1\rangle &= \alpha_p \alpha_{e_1} \alpha_{e_2} |R\rangle |\uparrow\uparrow\rangle_{12} + \alpha_p \alpha_{e_1} \beta_{e_2} |R\rangle |\uparrow\downarrow\rangle_{12} \\ &\quad + \alpha_p \beta_{e_1} \alpha_{e_2} |R\rangle |\downarrow\uparrow\rangle_{12} + \alpha_p \beta_{e_1} \beta_{e_2} |R\rangle |\downarrow\downarrow\rangle_{12} \\ &\quad + \beta_p \alpha_{e_1} \alpha_{e_2} |L^\uparrow\rangle |\uparrow\uparrow\rangle_{12} + \beta_p \alpha_{e_1} \beta_{e_2} |L^\uparrow\rangle |\uparrow\downarrow\rangle_{12} \\ &\quad + \beta_p \beta_{e_1} \alpha_{e_2} |L^\uparrow\rangle |\downarrow\uparrow\rangle_{12} + \beta_p \beta_{e_1} \beta_{e_2} |L^\uparrow\rangle |\downarrow\downarrow\rangle_{12}. \end{aligned} \quad (13)$$

The photon in the state  $|L^\uparrow\rangle$  is injected into cavity 1 and interacts with the QD inside the microcavity. This nonlinear interaction makes the state of the system be changed as

$$\begin{aligned} |\Phi_2\rangle &= \alpha_p \alpha_{e_1} \alpha_{e_2} |R\rangle |\uparrow\uparrow\rangle_{12} + \alpha_p \alpha_{e_1} \beta_{e_2} |R\rangle |\uparrow\downarrow\rangle_{12} \\ &\quad + \alpha_p \beta_{e_1} \alpha_{e_2} |R\rangle |\downarrow\uparrow\rangle_{12} + \alpha_p \beta_{e_1} \beta_{e_2} |R\rangle |\downarrow\downarrow\rangle_{12} \\ &\quad - \beta_p \alpha_{e_1} \alpha_{e_2} |L^\uparrow\rangle |\uparrow\uparrow\rangle_{12} - \beta_p \alpha_{e_1} \beta_{e_2} |L^\uparrow\rangle |\uparrow\downarrow\rangle_{12} \\ &\quad + \beta_p \beta_{e_1} \alpha_{e_2} |R^\downarrow\rangle |\downarrow\uparrow\rangle_{12} + \beta_p \beta_{e_1} \beta_{e_2} |R^\downarrow\rangle |\downarrow\downarrow\rangle_{12}. \end{aligned} \quad (14)$$

Whether the photon is in the state  $|L^\uparrow\rangle$  from path 3 or the photon is in the state  $|R^\downarrow\rangle$  from path 4, it will be emerged in spatial mode 5 by  $PBS_2$ . Before the photon from path 5 passes through  $PBS_3$  and then is injected into cavity 2, an  $H_p$  operation is performed on it (i.e., passing through the HWP), and an  $H_e$  operation is also performed on the electron in cavity 2. That is, before the photon interacts with the QD in cavity 2, the state

of the system becomes

$$\begin{aligned}
|\Phi_3\rangle &= \alpha_p \alpha_{e_1} \alpha_{e_2} |R\rangle |\uparrow\rightarrow\rangle_{12} + \alpha_p \alpha_{e_1} \beta_{e_2} |R\rangle |\uparrow\leftarrow\rangle_{12} \\
&+ \alpha_p \beta_{e_1} \alpha_{e_2} |R\rangle |\downarrow\rightarrow\rangle_{12} + \alpha_p \beta_{e_1} \beta_{e_2} |R\rangle |\downarrow\leftarrow\rangle_{12} \\
&- \frac{1}{2} \beta_p \alpha_{e_1} \alpha_{e_2} (|R^\downarrow\rangle - |L^\uparrow\rangle) |\uparrow\rangle_1 (|\uparrow\rangle + |\downarrow\rangle)_2 \\
&- \frac{1}{2} \beta_p \alpha_{e_1} \beta_{e_2} (|R^\downarrow\rangle - |L^\uparrow\rangle) |\uparrow\rangle_1 (|\uparrow\rangle - |\downarrow\rangle)_2 \\
&+ \frac{1}{2} \beta_p \beta_{e_1} \alpha_{e_2} (|R^\downarrow\rangle + |L^\uparrow\rangle) |\downarrow\rangle_1 (|\uparrow\rangle + |\downarrow\rangle)_2 \\
&+ \frac{1}{2} \beta_p \beta_{e_1} \beta_{e_2} (|R^\downarrow\rangle + |L^\uparrow\rangle) |\downarrow\rangle_1 (|\uparrow\rangle - |\downarrow\rangle)_2. \quad (15)
\end{aligned}$$

The nonlinear interaction between the photon and the QD inside cavity 2 makes the state given by Eq.(15) become

$$\begin{aligned}
|\Phi_4\rangle &= \alpha_p \alpha_{e_1} \alpha_{e_2} |R\rangle |\uparrow\rightarrow\rangle_{12} + \alpha_p \alpha_{e_1} \beta_{e_2} |R\rangle |\uparrow\leftarrow\rangle_{12} \\
&+ \alpha_p \beta_{e_1} \alpha_{e_2} |R\rangle |\downarrow\rightarrow\rangle_{12} + \alpha_p \beta_{e_1} \beta_{e_2} |R\rangle |\downarrow\leftarrow\rangle_{12} \\
&+ \frac{1}{2} \beta_p \alpha_{e_1} \alpha_{e_2} (|R^\downarrow\rangle - |L^\uparrow\rangle) |\uparrow\rangle_1 (|\uparrow\rangle + |\downarrow\rangle)_2 \\
&+ \frac{1}{2} \beta_p \alpha_{e_1} \beta_{e_2} (|R^\downarrow\rangle - |L^\uparrow\rangle) |\uparrow\rangle_1 (|\uparrow\rangle - |\downarrow\rangle)_2 \\
&- \frac{1}{2} \beta_p \beta_{e_1} \alpha_{e_2} (|R^\downarrow\rangle + |L^\uparrow\rangle) |\downarrow\rangle_1 (|\uparrow\rangle - |\downarrow\rangle)_2 \\
&- \frac{1}{2} \beta_p \beta_{e_1} \beta_{e_2} (|R^\downarrow\rangle + |L^\uparrow\rangle) |\downarrow\rangle_1 (|\uparrow\rangle + |\downarrow\rangle)_2. \quad (16)
\end{aligned}$$

Next, an  $H_p$  operation (i.e., the HWP in path 8) is performed on the photon in the state  $|R^\downarrow\rangle$  or the photon in the state  $|L^\uparrow\rangle$  coming from paths 7 and 6, respectively, and an  $H_e$  operation is also performed on the electron in cavity 2. After these two operations, the state of the system becomes

$$\begin{aligned}
|\Phi_5\rangle &= \alpha_p \alpha_{e_1} \alpha_{e_2} |R\rangle |\uparrow\uparrow\rangle_{12} + \alpha_p \alpha_{e_1} \beta_{e_2} |R\rangle |\uparrow\downarrow\rangle_{12} \\
&+ \alpha_p \beta_{e_1} \alpha_{e_2} |R\rangle |\downarrow\uparrow\rangle_{12} + \alpha_p \beta_{e_1} \beta_{e_2} |R\rangle |\downarrow\downarrow\rangle_{12} \\
&+ \beta_p \alpha_{e_1} \alpha_{e_2} |L^\uparrow\rangle |\uparrow\uparrow\rangle_{12} + \beta_p \alpha_{e_1} \beta_{e_2} |L^\uparrow\rangle |\uparrow\downarrow\rangle_{12} \\
&- \beta_p \beta_{e_1} \alpha_{e_2} |R^\downarrow\rangle |\downarrow\downarrow\rangle_{12} - \beta_p \beta_{e_1} \beta_{e_2} |R^\downarrow\rangle |\downarrow\uparrow\rangle_{12}. \quad (17)
\end{aligned}$$

After the photon passes through the HWP in spatial mode 8, it is led back to cavity 1. Before the photon reaches PBS<sub>4</sub>, it passes through a phase shifter  $P_\pi$ .  $P_\pi$  makes  $|R^\downarrow\rangle$  and  $|L^\uparrow\rangle$  in Eq.(17) become  $-|R^\downarrow\rangle$  and  $-|L^\uparrow\rangle$ , respectively. When the photon passes through cavity 1, the nonlinear interaction between the photon and the QD in cavity 1 induces the state of the system to be

$$\begin{aligned}
|\Phi_6\rangle &= \alpha_p \alpha_{e_1} \alpha_{e_2} |R\rangle |\uparrow\uparrow\rangle_{12} + \alpha_p \alpha_{e_1} \beta_{e_2} |R\rangle |\uparrow\downarrow\rangle_{12} \\
&+ \alpha_p \beta_{e_1} \alpha_{e_2} |R\rangle |\downarrow\uparrow\rangle_{12} + \alpha_p \beta_{e_1} \beta_{e_2} |R\rangle |\downarrow\downarrow\rangle_{12} \\
&+ \beta_p \alpha_{e_1} \alpha_{e_2} |L^\uparrow\rangle |\uparrow\uparrow\rangle_{12} + \beta_p \alpha_{e_1} \beta_{e_2} |L^\uparrow\rangle |\uparrow\downarrow\rangle_{12} \\
&+ \beta_p \beta_{e_1} \alpha_{e_2} |L^\uparrow\rangle |\downarrow\downarrow\rangle_{12} + \beta_p \beta_{e_1} \beta_{e_2} |L^\uparrow\rangle |\downarrow\uparrow\rangle_{12}. \quad (18)
\end{aligned}$$

When the photon in the state  $|L^\uparrow\rangle$  coming from cavity 1 passes through PBS<sub>4</sub> again, it is reflected to PBS<sub>5</sub>. When

the two wavepackets from spatial modes 1 and 11 pass through PBS<sub>5</sub> simultaneously, the system composed of the photon and the two electrons is in the state

$$\begin{aligned}
|\Phi_7\rangle &= \alpha_p \alpha_{e_1} |R\rangle |\uparrow\rangle_1 (\alpha_{e_2} |\uparrow\rangle + \beta_{e_2} |\downarrow\rangle)_2 \\
&+ \alpha_p \beta_{e_1} |R\rangle |\downarrow\rangle_1 (\alpha_{e_2} |\uparrow\rangle + \beta_{e_2} |\downarrow\rangle)_2 \\
&+ \beta_p \alpha_{e_1} |L\rangle |\uparrow\rangle_1 (\alpha_{e_2} |\uparrow\rangle + \beta_{e_2} |\downarrow\rangle)_2 \\
&+ \beta_p \beta_{e_1} |L\rangle |\downarrow\rangle_1 (\alpha_{e_2} |\downarrow\rangle + \beta_{e_2} |\uparrow\rangle)_2. \quad (19)
\end{aligned}$$

From Eq.(19), one can see that the state of the target qubit (i.e., the electron spin  $e_2$  in cavity 2) is flipped when the flying photon  $p$  is in the state  $|L\rangle$  and the control electron-spin qubit  $e_1$  is in the state  $|\downarrow\rangle_1$ , compared to the state shown in Eq.(12). Otherwise, it does not change. That is, the quantum circuit shown in Fig.3 can be used to construct a Toffoli gate on a three-qubit hybrid system, by using the flying photon and the electron confined in the first optical microcavity as the two control qubits and using the electron confined in the second microcavity as the target qubit. In principle, this Toffoli gate has a success probability of 100%. It is a deterministic three-qubit gate.

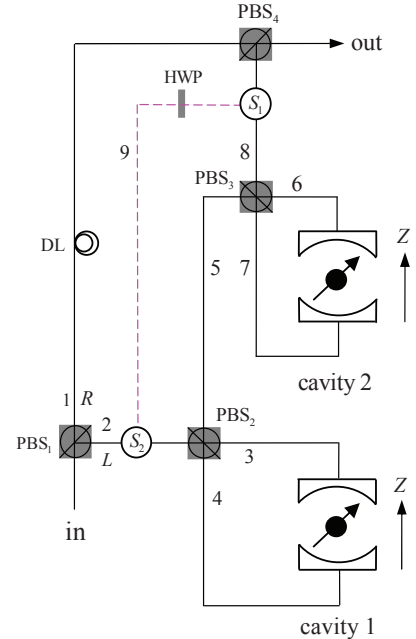


FIG. 4: (Color online) Schematic setup for a deterministic three-qubit Fredkin gate with a flying photon polarization as the control qubit and two confined electron spins as the target qubits.  $S_1$  and  $S_2$  are two optical switches.

## V. FREDKIN GATE ON A THREE-QUBIT HYBRID SYSTEM

The matrix representation of the three-qubit Fredkin gate can be written as

$$U_F = \text{diag} \left\{ I_4, \begin{pmatrix} 1 & 0 & 0 & 0 \\ 0 & 0 & 1 & 0 \\ 0 & 1 & 0 & 0 \\ 0 & 0 & 0 & 1 \end{pmatrix} \right\}, \quad (20)$$

in the basis  $\{|R\rangle|\uparrow\uparrow\rangle_{12}, |R\rangle|\uparrow\downarrow\rangle_{12}, |R\rangle|\downarrow\uparrow\rangle_{12}, |R\rangle|\downarrow\downarrow\rangle_{12}, |L\rangle|\uparrow\uparrow\rangle_{12}, |L\rangle|\uparrow\downarrow\rangle_{12}, |L\rangle|\downarrow\uparrow\rangle_{12}, |L\rangle|\downarrow\downarrow\rangle_{12}\}$ . Here  $I_4$  is the four-dimensional unit matrix. That is, the gate implements a swap operation on two stationary electron-spin qubits when the control qubit (the flying photon  $p$ ) is in the state  $|L\rangle$ . Otherwise, it does nothing.

Now, let us discuss how to construct this three-qubit gate. Its schematic setup is shown in Fig.4. Suppose that the initial state of the flying photon and the two stationary electrons confined in the two QDs inside two microcavities (cavity 1 and cavity 2) are  $|\psi\rangle_p = \alpha_c|R\rangle + \beta_c|L\rangle$  and  $|\psi\rangle_{e_i} = \alpha_{t_i}|\uparrow\rangle_i + \beta_{t_i}|\downarrow\rangle_i$  (here  $i = 1, 2$ , and  $|\alpha_c|^2 + |\beta_c|^2 = |\alpha_{t_i}|^2 + |\beta_{t_i}|^2 = 1$ ), respectively. That is, the initial state of the whole system composed of a photon and two electron spins can be written as

$$\begin{aligned} |\Omega_0\rangle &= |\psi\rangle_p \otimes |\psi\rangle_{e_1} \otimes |\psi\rangle_{e_2}, \\ &= |\Omega'_0\rangle + |\Omega''_0\rangle. \end{aligned} \quad (21)$$

Here

$$\begin{aligned} |\Omega'_0\rangle &= \alpha_c\alpha_{t_1}\alpha_{t_2}|R\rangle|\uparrow\uparrow\rangle_{12} + \alpha_c\alpha_{t_1}\beta_{t_2}|R\rangle|\uparrow\downarrow\rangle_{12} \\ &\quad + \alpha_c\beta_{t_1}\alpha_{t_2}|R\rangle|\downarrow\uparrow\rangle_{12} + \alpha_c\beta_{t_1}\beta_{t_2}|R\rangle|\downarrow\downarrow\rangle_{12}, \\ |\Omega''_0\rangle &= \beta_c\alpha_{t_1}\alpha_{t_2}|L\rangle|\uparrow\uparrow\rangle_{12} + \beta_c\alpha_{t_1}\beta_{t_2}|L\rangle|\uparrow\downarrow\rangle_{12} \\ &\quad + \beta_c\beta_{t_1}\alpha_{t_2}|L\rangle|\downarrow\uparrow\rangle_{12} + \beta_c\beta_{t_1}\beta_{t_2}|L\rangle|\downarrow\downarrow\rangle_{12}. \end{aligned} \quad (22)$$

Our scheme for a three-qubit Fredkin gate (see Fig.4) consists of three parts (three rounds).

(i) The injecting photon is split into two wave-packets by  $\text{PBS}_1$ , that is, the part in the state  $|R\rangle$  and that in the state  $|L\rangle$ . The photon in the state  $|R\rangle$  does not pass through the cavities, while the photon in the state  $|L\rangle$  is injected into the cavities. Before the photon in the state  $|L\rangle$  reaches  $\text{PBS}_2$ , the state of the three-qubit hybrid system given by Eq.(21) changes to be

$$|\Omega_1\rangle = |\Omega'_0\rangle + |\Omega''_1\rangle, \quad (23)$$

with

$$\begin{aligned} |\Omega''_1\rangle &= \beta_c\alpha_{t_1}\alpha_{t_2}|L^\uparrow\rangle|\uparrow\uparrow\rangle_{12} + \beta_c\alpha_{t_1}\beta_{t_2}|L^\uparrow\rangle|\uparrow\downarrow\rangle_{12} \\ &\quad + \beta_c\beta_{t_1}\alpha_{t_2}|L^\uparrow\rangle|\downarrow\uparrow\rangle_{12} + \beta_c\beta_{t_1}\beta_{t_2}|L^\uparrow\rangle|\downarrow\downarrow\rangle_{12}. \end{aligned} \quad (24)$$

Since the photon in the state  $|R\rangle$  does not pass through the cavities,  $|\Omega'_0\rangle$  stays the same all the time and only  $|\Omega''_0\rangle$  is changed. The nonlinear interaction between the

photon and the QD inside cavity 1 makes  $|\Omega''_1\rangle$  be changed as

$$\begin{aligned} |\Omega''_1\rangle &= -\beta_c\alpha_{t_1}\alpha_{t_2}|L^\uparrow\rangle|\uparrow\uparrow\rangle_{12} - \beta_c\alpha_{t_1}\beta_{t_2}|L^\uparrow\rangle|\uparrow\downarrow\rangle_{12} \\ &\quad + \beta_c\beta_{t_1}\alpha_{t_2}|R^\downarrow\rangle|\downarrow\uparrow\rangle_{12} + \beta_c\beta_{t_1}\beta_{t_2}|R^\downarrow\rangle|\downarrow\downarrow\rangle_{12}. \end{aligned} \quad (25)$$

After the photon interacts with the QD inside cavity 1, the emitting photon emerges in spatial mode 5. Next, the photon coming from path 5 is injected into cavity 2. After the photon interacts with the QD inside cavity 2,  $|\Omega''_2\rangle$  becomes

$$\begin{aligned} |\Omega''_2\rangle &= \beta_c\alpha_{t_1}\alpha_{t_2}|L^\uparrow\rangle|\uparrow\uparrow\rangle_{12} - \beta_c\alpha_{t_1}\beta_{t_2}|R^\downarrow\rangle|\uparrow\downarrow\rangle_{12} \\ &\quad - \beta_c\beta_{t_1}\alpha_{t_2}|R^\downarrow\rangle|\downarrow\uparrow\rangle_{12} + \beta_c\beta_{t_1}\beta_{t_2}|L^\uparrow\rangle|\downarrow\downarrow\rangle_{12}. \end{aligned} \quad (26)$$

After the photon interacts with the QD inside cavity 2, it is emitted from path 8 whether it is in the state  $|R^\downarrow\rangle$  and comes from path 7 or it is in the state  $|L^\uparrow\rangle$  and comes from path 6. Therefore, after the first round, the state of the whole system becomes

$$\begin{aligned} |\Omega_2\rangle &= |\Omega'_1\rangle + |\Omega''_2\rangle, \\ &= \alpha_c\alpha_{t_1}\alpha_{t_2}|R\rangle|\uparrow\uparrow\rangle_{12} + \alpha_c\alpha_{t_1}\beta_{t_2}|R\rangle|\uparrow\downarrow\rangle_{12} \\ &\quad + \alpha_c\beta_{t_1}\alpha_{t_2}|R\rangle|\downarrow\uparrow\rangle_{12} + \alpha_c\beta_{t_1}\beta_{t_2}|R\rangle|\downarrow\downarrow\rangle_{12} \\ &\quad + \beta_c\alpha_{t_1}\alpha_{t_2}|L^\uparrow\rangle|\uparrow\uparrow\rangle_{12} - \beta_c\alpha_{t_1}\beta_{t_2}|R^\downarrow\rangle|\uparrow\downarrow\rangle_{12} \\ &\quad - \beta_c\beta_{t_1}\alpha_{t_2}|R^\downarrow\rangle|\downarrow\uparrow\rangle_{12} + \beta_c\beta_{t_1}\beta_{t_2}|L^\uparrow\rangle|\downarrow\downarrow\rangle_{12}. \end{aligned} \quad (27)$$

Combing Eqs.(21)and (26) and Fig.4, one can find that the effect of this round can be described by a unitary matrix  $U$ ,

$$U = \begin{pmatrix} 1 & 0 & 0 & 0 & 0 & 0 & 0 & 0 \\ 0 & 0 & 0 & 0 & 0 & -1 & 0 & 0 \\ 0 & 0 & 0 & 0 & 0 & 0 & -1 & 0 \\ 0 & 0 & 0 & 1 & 0 & 0 & 0 & 0 \\ 0 & 0 & 0 & 0 & 1 & 0 & 0 & 0 \\ 0 & -1 & 0 & 0 & 0 & 0 & 0 & 0 \\ 0 & 0 & -1 & 0 & 0 & 0 & 0 & 0 \\ 0 & 0 & 0 & 0 & 0 & 0 & 0 & 1 \end{pmatrix}, \quad (28)$$

in the basis  $\{|R^\downarrow\rangle|\uparrow\uparrow\rangle_{12}, |R^\downarrow\rangle|\uparrow\downarrow\rangle_{12}, |R^\downarrow\rangle|\downarrow\uparrow\rangle_{12}, |R^\downarrow\rangle|\downarrow\downarrow\rangle_{12}, |L^\uparrow\rangle|\uparrow\uparrow\rangle_{12}, |L^\uparrow\rangle|\uparrow\downarrow\rangle_{12}, |L^\uparrow\rangle|\downarrow\uparrow\rangle_{12}, |L^\uparrow\rangle|\downarrow\downarrow\rangle_{12}\}$  as  $|\Omega''_3\rangle = U|\Omega''_2\rangle$  and  $\Omega'_0$  keeps the same one all the time.

(ii) We lead the photon emitting from spatial mode 8 back to cavity 1 by using the optical switches  $S_1$  and  $S_2$  (dashed line). After the second round, the photon emitting from spatial mode 8 is led back to cavity 1 again for the third round. Before and after the second round, an  $H_p$  operation (i.e., an HWP in path 9) is performed on the photon emitting from spatial mode 8, and an  $H_e$  operation is also performed on each of the electrons in cavities 1 and 2. Hence, before the third round, the state of the whole system is changed to be

$$|\Omega_3\rangle = |\Omega'_1\rangle$$

$$\begin{aligned}
& + ((H_p \otimes H_e \otimes H_e) \cdot U \cdot (H_p \otimes H_e \otimes H_e))|\Omega_3'\rangle, \\
& = \alpha_c \alpha_{t_1} \alpha_{t_2} |R\rangle |\uparrow\uparrow\rangle_{12} + \alpha_c \alpha_{t_1} \beta_{t_2} |R\rangle |\uparrow\downarrow\rangle_{12} \\
& + \alpha_c \beta_{t_1} \alpha_{t_2} |R\rangle |\downarrow\uparrow\rangle_{12} + \alpha_c \beta_{t_1} \beta_{t_2} |R\rangle |\downarrow\downarrow\rangle_{12} \\
& + \beta_c \alpha_{t_1} \alpha_{t_2} |L^\uparrow\rangle |\uparrow\uparrow\rangle_{12} - \beta_c \alpha_{t_1} \beta_{t_2} |R^\downarrow\rangle |\downarrow\uparrow\rangle_{12} \\
& - \beta_c \beta_{t_1} \alpha_{t_2} |R^\downarrow\rangle |\uparrow\downarrow\rangle_{12} + \beta_c \beta_{t_1} \beta_{t_2} |L^\uparrow\rangle |\downarrow\downarrow\rangle_{12}.
\end{aligned} \tag{29}$$

(iii) After the third round, the state of the whole system becomes

$$\begin{aligned}
|\Omega_4\rangle & = |\Omega_1'\rangle \\
& + U(\beta_c \alpha_{t_1} \alpha_{t_2} |L^\uparrow\rangle |\uparrow\uparrow\rangle_{12} - \beta_c \alpha_{t_1} \beta_{t_2} |R^\downarrow\rangle |\downarrow\uparrow\rangle_{12} \\
& - \beta_c \beta_{t_1} \alpha_{t_2} |R^\downarrow\rangle |\uparrow\downarrow\rangle_{12} + \beta_c \beta_{t_1} \beta_{t_2} |L^\uparrow\rangle |\downarrow\downarrow\rangle_{12}), \\
& = \alpha_c \alpha_{t_1} \alpha_{t_2} |R\rangle |\uparrow\uparrow\rangle_{12} + \alpha_c \alpha_{t_1} \beta_{t_2} |R\rangle |\uparrow\downarrow\rangle_{12} \\
& + \alpha_c \beta_{t_1} \alpha_{t_2} |R\rangle |\downarrow\uparrow\rangle_{12} + \alpha_c \beta_{t_1} \beta_{t_2} |R\rangle |\downarrow\downarrow\rangle_{12} \\
& + \beta_c \alpha_{t_1} \alpha_{t_2} |L^\uparrow\rangle |\uparrow\uparrow\rangle_{12} + \beta_c \alpha_{t_1} \beta_{t_2} |L^\uparrow\rangle |\downarrow\uparrow\rangle_{12} \\
& + \beta_c \beta_{t_1} \alpha_{t_2} |L^\uparrow\rangle |\uparrow\downarrow\rangle_{12} + \beta_c \beta_{t_1} \beta_{t_2} |L^\uparrow\rangle |\downarrow\downarrow\rangle_{12}.
\end{aligned} \tag{30}$$

When the two wavepackets from spatial modes 1 and 8 pass through PBS<sub>4</sub> simultaneously, the system composed of the photon and the two electrons is in the state

$$\begin{aligned}
|\Omega_5\rangle & = \alpha_c |R\rangle (\alpha_{t_1} |\uparrow\rangle + \beta_{t_1} |\downarrow\rangle)_1 (\alpha_{t_2} |\uparrow\rangle + \beta_{t_2} |\downarrow\rangle)_2 \\
& + \beta_c |L\rangle (\alpha_{t_2} |\uparrow\rangle + \beta_{t_2} |\downarrow\rangle)_1 (\alpha_{t_1} |\uparrow\rangle + \beta_{t_1} |\downarrow\rangle)_2.
\end{aligned} \tag{31}$$

From Eq.(31), one can see that the states of the two solid-state target qubits (the two electron spins in cavities 1 and 2) are swapped when the photon qubit is in the state  $|L\rangle$ , while they do not swap when the photon qubit is in the state  $|R\rangle$ . The quantum circuit shown in Fig.4 can be used to construct the Fredkin gate on a three-qubit hybrid system in a deterministic way.

## VI. FIDELITIES AND EFFICIENCIES OF THE GATES

A crucial component in our schemes for deterministic hybrid quantum gates is the  $X^-$ -cavity system. The quantum circuits aforementioned for hybrid quantum gates are all under the ideal case in which the success probability for each gate is 100% in principle. Here, we assume that the Hadamard operation on the electron is perfect as the spin manipulation technique is well developed by using pulsed magnetic-resonance, nanosecond microwave pulse, or picosecond/femtosecond optical pulse techniques [25, 26, 39, 40]. The optical elements, such as PBS, HWP, and optical switches, are also assumed to be perfect, that is, the yield of the photon is 100%. In a realistic  $X^-$ -cavity system, the side leakage should be taken into account, and it affects the success probability of the device. The whole process can be represented by the Heisenberg equations of motion and the

input-output relations [41]

$$\begin{aligned}
\frac{d\hat{a}}{dt} & = -\left[i(\omega_c - \omega) + \kappa + \frac{\kappa_s}{2}\right] \hat{a} - g\sigma_- \\
& \quad - \sqrt{\kappa} \hat{a}_{in} - \sqrt{\kappa} \hat{a}'_{in} + \hat{H}, \\
\frac{d\sigma_-}{dt} & = -\left[i(\omega_{X^-} - \omega) + \frac{\gamma}{2}\right] \sigma_- - g\sigma_z \hat{a} + \hat{G}, \\
\hat{a}_r & = \hat{a}_{in} + \sqrt{\kappa} \hat{a}, \\
\hat{a}_t & = \hat{a}'_{in} + \sqrt{\kappa} \hat{a}.
\end{aligned} \tag{32}$$

Here  $\hat{a}$  and  $\sigma_-$  are the cavity field operator and the  $X^-$  dipole operator, respectively.  $\hat{H}$  and  $\hat{G}$  are the noise operators related to the reservoirs.  $\hat{a}_{in}$  and  $\hat{a}'_{in}$  are the two input field operators, shown in Fig.1.  $\hat{a}_r$  and  $\hat{a}_t$  are the two output field operators.  $\omega$ ,  $\omega_c$ , and  $\omega_{X^-}$  are the frequencies of the input photon, the cavity mode, and the  $X^-$  transition, respectively.  $\gamma/2$  and  $\kappa$  ( $\kappa_s/2$ ) are the dipole decay rate and the cavity field decay rate (the side leakage rate), respectively.  $g$  is the coupling strength between  $X^-$  and the cavity mode. By taking a weak approximation, the reflection and the transmission coefficients of the  $X^-$ -cavity system  $r(\omega)$  and  $t(\omega)$  can be obtained as [28]

$$\begin{aligned}
r(\omega) & = 1 + t(\omega), \\
t(\omega) & = \frac{-\kappa[i(\omega_{X^-} - \omega) + \frac{\gamma}{2}]}{[i(\omega_{X^-} - \omega) + \frac{\gamma}{2}][i(\omega_c - \omega) + \kappa + \frac{\kappa_s}{2}] + g^2}.
\end{aligned} \tag{33}$$

In our works, we consider  $\omega_{X^-} = \omega_c = \omega$ , and the reflection and the transmission coefficients of the uncoupled cavity (cold cavity, described with the subscript 0) and the coupled cavity (hot cavity) can be simplified as

$$r_0(\omega) = \frac{\frac{\kappa_s}{2}}{\kappa + \frac{\kappa_s}{2}}, \quad t_0(\omega) = -\frac{\kappa}{\kappa + \frac{\kappa_s}{2}}, \tag{34}$$

and

$$r(\omega) = 1 + t(\omega), \quad t(\omega) = -\frac{\frac{\gamma}{2}\kappa}{\frac{\gamma}{2}[\kappa + \frac{\kappa_s}{2}] + g^2}, \tag{35}$$

respectively. The rules for optical transitions in a realistic  $X^-$ -cavity system become [28, 29]

$$\begin{aligned}
|R^\downarrow \downarrow\rangle & \rightarrow |r||L^\uparrow \downarrow\rangle + |t||R^\downarrow \downarrow\rangle, \\
|L^\uparrow \downarrow\rangle & \rightarrow |r||R^\downarrow \downarrow\rangle + |t||L^\uparrow \downarrow\rangle, \\
|R^\downarrow \uparrow\rangle & \rightarrow -|t_0||R^\downarrow \uparrow\rangle - |r_0||L^\uparrow \uparrow\rangle, \\
|L^\uparrow \uparrow\rangle & \rightarrow -|t_0||L^\uparrow \uparrow\rangle - |r_0||R^\downarrow \uparrow\rangle.
\end{aligned} \tag{36}$$

From Eq.(36), one can find that the reflection and the transmission coefficients connect to the fidelities and efficiencies of our universal quantum gates. Substituting Eq.(1) with Eq.(36), and combing the arguments made in Sec.III, we find that the state of the system described by Eq.(8) becomes

$$|\Psi_4'\rangle = \alpha_c \alpha_t |R\rangle |\uparrow\rangle + \alpha_c \beta_t |R\rangle |\downarrow\rangle$$



$$\begin{aligned}
& + \frac{\beta_c \alpha_t}{2} (|t_0\rangle + |r_0\rangle - |t\rangle - |r\rangle) |L\rangle | \uparrow \rangle \\
& + \frac{\beta_c \alpha_t}{2} (|t_0\rangle + |r_0\rangle + |t\rangle + |r\rangle) |L\rangle | \downarrow \rangle \\
& + \frac{\beta_c \beta_t}{2} (|t_0\rangle + |r_0\rangle + |t\rangle + |r\rangle) |L\rangle | \uparrow \rangle \\
& + \frac{\beta_c \beta_t}{2} (|t_0\rangle + |r_0\rangle - |t\rangle - |r\rangle) |L\rangle | \downarrow \rangle. \quad (37)
\end{aligned}$$

The terms with underlines indicate the states which take the bit-flip error.

Defining the fidelity of a quantum gate as  $F = |\langle \Psi_r | \Psi_i \rangle|^2$ . Here  $|\Psi_r\rangle$  and  $|\Psi_i\rangle$  are the final states of the hybrid system in our schemes for quantum gates in the realistic condition and the ideal condition, respectively. Therefore, the fidelity of our CNOT gate on the two-qubit hybrid system discussed in Sec.III can be written as

$$F_{CNOT} = \left[ \frac{1 + |t_0| + |r_0|}{2} \right]^2 = 1. \quad (38)$$

Similar calculations can be done for the Toffoli and the Fredkin gates on the three-qubit hybrid system discussed in Secs. IV and V, respectively. That is, the fidelities of the Toffoli and the Fredkin gates  $F_T$  and  $F_F$  can be expressed as

$$F_T = \frac{1}{16} [2 + |r_0| (|r|^2 - |t|^2 + |r_0|^2 + |t_0|^2) + |t_0| (1 + |r_0|^2 + |t_0|^2)]^2, \quad (39)$$

$$\begin{aligned}
F_F &= \frac{1}{64} [4 + (1 + (|r_0| - |t|)(|r| - |t_0|)) \\
&\times (|r| + |r_0| - |t| - |t_0|)(|r| - |r_0| - |t| + |t_0|) \\
&+ 2(|r| + |r_0|)(|t| + |t_0|) \\
&+ \frac{1}{2}((|r| - |t|)^2 + (|r_0| - |t_0|)^2) \\
&\times ((|r| + |r_0|)^2 + (|t| + |t_0|)^2)]^2. \quad (40)
\end{aligned}$$

Defining the efficiency of a quantum gate as the ratio of the number of the outputting photons to the inputting photons. The efficiency is also determined by the reflection and the transmission coefficients of the  $X^-$ -cavity system. The efficiencies of these gates can be written as

$$\begin{aligned}
\eta_{CNOT} &= \frac{1}{2} \left( 1 + \frac{|r|^2 + |t|^2 + |r_0|^2 + |t_0|^2}{2} \right), \\
\eta_T &= \frac{1}{2} \left[ 1 + \left( \frac{|r|^2 + |t|^2 + |r_0|^2 + |t_0|^2}{2} \right)^3 \right], \\
\eta_F &= \frac{1}{2} \left[ 1 + \left( \frac{|r|^2 + |t|^2 + |r_0|^2 + |t_0|^2}{2} \right)^6 \right]. \quad (41)
\end{aligned}$$

It is still a big challenge to achieve strong coupling in experiments. However, strong coupling has been demonstrated in various microcavity- and nanocavity-QD systems recently [42–46].  $g/(\kappa + \kappa_s) \simeq 0.5$  for micropillar

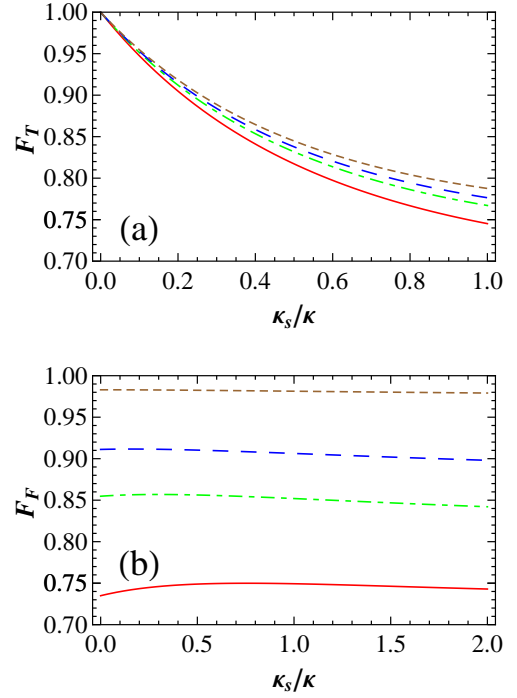


FIG. 5: (Color online) The fidelities of our three-qubit gates vs the side leakage rate  $\kappa_s/\kappa$  and the coupling strength  $g/\kappa$ . (a) The fidelity of our Toffoli gate ( $F_T$ ). (b) The fidelity of our Fredkin gate ( $F_F$ ). The solid (red), dashed-dotted (green), large-dashed (blue), and dashed (brown) lines correspond to  $g = 0.5\kappa$ ,  $g = 0.75\kappa$ ,  $g = 1.0\kappa$ , and  $g = 2.4\kappa$ , respectively.  $\gamma = 0.1\kappa$  which is experimentally achievable and  $\omega_{X^-} = \omega_c = \omega$  are taken here.

microcavities with a diameter of  $1.5 \mu\text{m}$  and a quality factor of  $Q = 8800$  have been reported [42].  $Q$  is dominated by  $\kappa$  and  $\kappa_s$ . For micropillar systems,  $Q$  can be increased to  $\sim 4 \times 10^4$  ( $g/(\kappa + \kappa_s) \simeq 2.4$ ) by improving the sample designs, growth, and fabrication [45]. By taking high- $Q$  micropillars and thinning down the top mirrors,  $Q$  can decrease to  $\sim 1.7 \times 10^4$  with  $\kappa_s/\kappa = 0.7$  and  $g/(\kappa + \kappa_s) \simeq 1.0$ , and the system remains in the strong coupling regime [31]. Recent experiments have indicated that the strong coupling can be achieved for  $d = 7.3 \mu\text{m}$  micropillars, where the side leakage is small compared with that of small micropillars [47].

The relations between the fidelities of our Toffoli gate or our Fredkin gate and the side leakage rate  $\kappa_s/\kappa$  and the coupling strength  $g/\kappa$  are shown in Fig.5. The efficiencies of our universal quantum gates are shown in Fig.6. For our schemes for hybrid quantum gates, in the weak regime, if  $g/\kappa = 0.5$  and  $\kappa_s/\kappa = 0.25$ ,  $F_T = 88.7\%$  and  $F_F = 74.5\%$  with  $\eta_{CNOT} = 88.2\%$ ,  $\eta_T = 72.4\%$ ,  $\eta_F = 60\%$ ; and  $F_T = 100\%$  and  $F_F = 73.5\%$  with  $\eta_{CNOT} = 93.1\%$ ,  $\eta_T = 81.9\%$ , and  $\eta_F = 70.4\%$  when  $\kappa_s/\kappa = 0$ . In the strong regime, when  $g/\kappa = 2.4$  and  $\kappa_s/\kappa = 0.5$ ,  $F_T = 84.5\%$  and  $F_F = 98.2\%$  with  $\eta_{CNOT} = 91.6\%$ ,  $\eta_T = 78.8\%$ , and  $\eta_F = 66.5\%$ . If



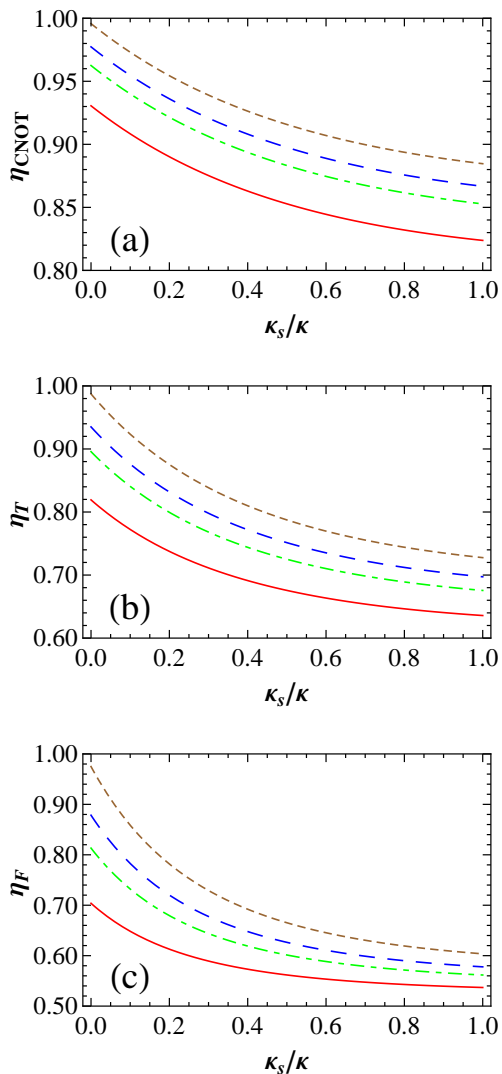


FIG. 6: (Color online) The efficiencies of our universal quantum gates vs the side leakage rate  $\kappa_s/\kappa$  and the coupling strength  $g/\kappa$ . (a) The efficiency of our CNOT gate ( $\eta_{CNOT}$ ). (b) The efficiency of our Toffoli gate ( $\eta_T$ ). (c) The efficiency of our Fredkin gate ( $\eta_F$ ). The solid (red), dashed-dotted (green), large-dashed (blue), and dashed (brown) lines correspond to  $g = 0.5\kappa$ ,  $g = 0.75\kappa$ ,  $g = 1.0\kappa$ , and  $g = 2.4\kappa$ , respectively. We take  $\gamma = 0.1\kappa$  and  $\omega_{X^-} = \omega_c = \omega$  for panels (a), (b), and (c).

the cavity leakage can be neglected, both the fidelity and the efficiency can reach near-unity ( $F_T = 100\%$  and  $F_F = 98.3\%$  with  $\eta_{CNOT} = 99.6\%$ ,  $\eta_T = 98.7\%$ , and  $\eta_F = 97.5\%$ ).  $F_T = 80.6\%$  and  $F_F = 90.9\%$  with  $\eta_{CNOT} = 88.2\%$ ,  $\eta_T = 72.2\%$ , and  $\eta_F = 59.9\%$  when  $g/\kappa = 1.0$  and  $\kappa_s/\kappa = 0.7$  ( $F_T = 100\%$  and  $F_F = 91.1\%$  with  $\eta_{CNOT} = 97.7\%$ ,  $\eta_T = 93.5\%$ , and  $\eta_F = 87.8\%$  when  $\kappa_s/\kappa = 0$ ). It is worth pointing out that  $g/\kappa$  and  $\kappa_s/\kappa$  does not affect the fidelity of our CNOT gate and it remains at unity.

Note that there are two kinds of exciton dephasing in the QD, the optical dephasing, and the spin dephasing

of  $X^-$ , caused by the exciton decoherence. Exciton dephasing reduces the fidelity by the amount of

$$[1 - \exp(-\tau/T_2)], \quad (42)$$

where  $\tau$  and  $T_2$  are the cavity photon lifetime and the trion coherence time, respectively. The optical dephasing reduces the fidelity less than 10% because the time scale of the excitons can reach hundreds of picoseconds [48–50], while the cavity photon lifetime is in the tens of picoseconds range for a self-assembled In(Ga)As-based QD with a cavity  $Q$  factor of  $10^4 - 10^5$  in the strong coupling regime. The effect of the spin dephasing can be neglected because the spin decoherence time ( $T_2^h > 100ns$ ) is several orders of magnitude longer than the cavity photon lifetime (typically  $\tau < 10ps$ ) [51–53].

In a realistic QD [e.g., for self-assembled In(Ga)As QDs], imperfect optical selection induced by heavy-light hole mixing reduces the fidelity by a few percent [54]. However, this undesirable mixing can be reduced by engineering the shape and the size of QDs or choosing the types of QDs.

## VII. DISCUSSION AND SUMMARY

We have proposed some schemes for implementing deterministic universal quantum logic gates between flying photon qubits and stationary electron-spin qubits with linear optical elements. Different from the work in Ref.[29] which presents a scheme for a CNOT gate with the confined electron as the control qubit and the photon as the target qubit, the CNOT gate in our work takes the flying photon as the control qubit and the electron as the target qubit. Compared with the two-qubit case, the works for implementing multi-qubit gates are generally quite complex and difficult. In this work, the schemes for constructing three-qubit universal quantum gates (Toffoli and Fredkin) in hybrid systems are also discussed.

The control qubit of the gates in our work is encoded on the photon which is easy to be manipulated. The target qubits are encoded on the electrons confined in QDs inside optical microcavities which can be used for processor and quantum computation. It is worth mentioning that our schemes require no additional qubits. This good feature reduces not only quantum resources but also errors. Since the electron-spin qubit is confined in a QD inside a double-sided microcavity, our gates are robust. The gate based on the single-sided QD-cavity system demands the transmission coefficient of the uncoupled cavity is balanceable with the reflection coefficient of the coupled cavity to get a high fidelity [28].

The cavity leakage and the cavity loss induce the bit-flip error and the different transmittance or reflectance between the hot cavity and the cold cavity in an  $X^-$ -cavity system. These factors reduce the fidelity and the efficiency of our gates. We have shown that a high fidelity and efficiency can be achieved in both the

weak coupling regime and in the strong coupling regime in our schemes. If the cavity leakage is much lower than the cavity loss (the ideal case), the fidelity and the efficiency of our gates can reach near-unity in the strong coupling regime.

### ACKNOWLEDGMENTS

This work is supported by the National Natural Science Foundation of China under Grant Nos. 10974020

and 11174039, NCET-11-0031, and the Fundamental Research Funds for the Central Universities.

- 
- [1] M. A. Nielsen and I. L. Chuang, *Quantum Computation and Quantum Information* (Cambridge University Press, Cambridge, UK, 2000).
- [2] A. Barenco, C. H. Bennett, R. Cleve, D. P. DiVincenzo, N. Margolus, P. Shor, T. Sleator, J. A. Smolin, and H. Weinfurter, *Phys. Rev. A* **52**, 3457 (1995).
- [3] G. Vidal and C. M. Dawson, *Phys. Rev. A* **69**, 010301 (2004).
- [4] F. Vatan and C. Williams, *Phys. Rev. A* **69**, 032315 (2004).
- [5] V. V. Shende, I. L. Markov, and S. S. Bullock, *Phys. Rev. A* **69**, 062321 (2004).
- [6] V. V. Shende, S. S. Bullock, I. L. Markov, *Phys. Rev. A* **70**, 012310 (2004).
- [7] Y. Y. Shi, *Quantum Inf. Comput.* **3**, 84 (2003).
- [8] E. Fredkin and T. Toffoli, *Int. J. Theor. Phys.* **21**, 219 (1982).
- [9] P. W. Shor, *SIAM J. Sci. Stat. Comput.* **26**, 1484 (1997).
- [10] D. G. Cory, M. D. Price, W. Maas, E. Knill, R. Laflamme, W. H. Zurek, T. F. Havel, and S. S. Somaroo, *Phys. Rev. Lett.* **81**, 2152 (1998).
- [11] E. Dennis, *Phys. Rev. A* **63**, 052314 (2001).
- [12] L. M. Liang and C. Z. Li, *Phys. Rev. A* **72**, 024303 (2005).
- [13] D. Loss and D. P. DiVincenzo, *Phys. Rev. A* **57**, 120 (1998).
- [14] A. Imamoglu, D. D. Awschalom, G. Burkard, D. P. DiVincenzo, D. Loss, M. Sherwin, and A. Small, *Phys. Rev. Lett.* **83**, 4204 (1999).
- [15] C. Piermarocchi, P. C. Chen, L. J. Sham, and D. G. Steel, *Phys. Rev. Lett.* **89**, 167402 (2002).
- [16] T. Calarco, A. Datta, P. Fedichev, E. Pazy, and P. Zoller, *Phys. Rev. A* **68**, 012310 (2003).
- [17] S. M. Clark, K. M. C. Fu, T. D. Ladd, and Y. Yamamoto, *Phys. Rev. Lett.* **99**, 040501 (2007).
- [18] Z. R. Lin, G. P. Guo, T. Tu, F. Y. Zhu, and G. C. Guo, *Phys. Rev. Lett.* **101**, 230501 (2008).
- [19] J. R. Petta, A. C. Johnson, J. M. Taylor, E. A. Laird, A. Yacoby, M. D. Lukin, C. M. Marcus, M. P. Hanson, and A. C. Gossard, *Science* **309**, 2180 (2005).
- [20] A. Greilich, D. R. Yakovlev, A. Shabaev, A. L. Efros, I. A. Yugova, R. Oulton, V. Stavarache, D. Reuter, A. Wieck, and M. Bayer, *Science* **313**, 341 (2006).
- [21] J. M. Elzerman, R. Hanson, L. H. Willems van Beveren, B. Witkamp, L. M. K. Vandersypen, and L. P. Kouwenhoven, *Nature (London)* **430**, 431 (2004).
- [22] M. Kroutvar, Y. Ducommun, D. Heiss, M. Bichler, D. Schuh, G. Abstreiter, and J. J. Finley, *Nature (London)* **432**, 81 (2004).
- [23] M. Atatüre, J. Dreiser, A. Badolato, A. Högele, K. Karrai, and A. Imamoglu, *Science* **312**, 551 (2006).
- [24] X. D. Xu, Y. W. Wu, B. Sun, Q. Huang, J. Cheng, D. G. Steel, A. S. Bracker, D. Gammon, C. Emary, and L. J. Sham, *Phys. Rev. Lett.* **99**, 097401 (2007).
- [25] J. Berezovsky, M. H. Mikkelsen, N. G. Stoltz, L. A. Coldren, and D. D. Awschalom, *Science* **320**, 349 (2008).
- [26] D. Press, T. D. Ladd, B. Y. Zhang, and Y. Yamamoto, *Nature (London)* **456**, 218 (2008).
- [27] C. Y. Hu, A. Young, J. L. O'Brien, W. J. Munro, and J. G. Rarity, *Phys. Rev. B* **78**, 085307 (2008).
- [28] C. Y. Hu, W. J. Munro, J. L. O'Brien, and J. G. Rarity, *Phys. Rev. B* **80**, 205326 (2009).
- [29] C. Bonato, F. Haupt, S. S. R. Oemrawsingh, J. Gudat, D. Ding, M. P. van Exter, and D. Bouwmeester, *Phys. Rev. Lett.* **104**, 160503 (2010).
- [30] C. Y. Hu, W. J. Munro, and J. G. Rarity, *Phys. Rev. B* **78**, 125318 (2008).
- [31] C. Y. Hu and J. G. Rarity, *Phys. Rev. B* **83**, 115303 (2011).
- [32] C. Wang, Y. Zhang, and G. S. Jin, *Phys. Rev. A* **84**, 032307 (2011).
- [33] T. Yu, A. D. Zhu, S. Zhang, K. H. Yeon, and S. C. Yu, *Phys. Scr.* **84**, 025001 (2011).
- [34] T. J. Wang, S. Y. Song, and G. L. Long, *Phys. Rev. A*, **85**, 062311 (2012).
- [35] B. C. Ren, H. R. Wei, M. Hua, T. Li, and F. G. Deng, *Opt. Express* **20**, 24664 (2012).
- [36] R. J. Warburton, C. S. Dürr, K. Karrai, J. P. Kotthaus, G. Medeiros-Ribeiro, and P. M. Petroff, *Phys. Rev. Lett.* **79**, 5282 (1997).
- [37] C. Y. Hu, W. Ossau, D. R. Yakovlev, and G. Landwehr, T. Wojtowicz, G. Karczewski, and J. Kossut, *Phys. Rev. B* **58**, R1766 (1998).
- [38] V. V. Shende and I. L. Markov, *Quant. Inf. Comput.* **9**, 461 (2009).
- [39] J. A. Gupta, R. Knobel, N. Samarth, and D. D. Awschalom, *Science* **292**, 2458 (2001).
- [40] P. C. Chen, C. Piermarocchi, L. J. Sham, D. Gammon, and D. G. Steel, *Phys. Rev. B* **69**, 075320 (2004).
- [41] D. F. Walls and G. J. Milburn, *Quantum Optics* (Springer-Verlag, Berlin, 1994).
- [42] J. P. Reithmaier, G. Sek, A. Löffler, C. Hofmann, S. Kuhn, S. Reitzenstein, L. V. Keldysh, V. D. Kulakovskii, T. L. Reinecke, and A. Forchel, *Nature (London)* **432**, 197 (2004).

- [43] T. Yoshie, A. Scherer, J. Hendrickson, G. Khitrova, H. M. Gibbs, G. Rupper, C. Ell, O. B. Shchekin, and D. G. Deppe, *Nature (London)* **432**, 200 (2004).
- [44] E. Peter, P. Senellart, D. Martrou, A. Lemaître, J. Hours, J. M. Gérard, and J. Bloch, *Phys. Rev. Lett.* **95**, 067401 (2005).
- [45] S. Reitzenstein, C. Hofmann, A. Gorbunov, M. Strauß, S. H. Kwon, C. Schneider, A. Löffler, S. Höfling, M. Kamp, and A. Forchel, *Appl. Phys. Lett.* **90**, 251109 (2007).
- [46] A. B. Young, R. Oulton, C. Y. Hu, A. C. T. Thijssen, C. Schneider, S. Reitzenstein, M. Kamp, S. Höfling, L. Worschech, A. Forchel, and J. G. Rarity, *Phys. Rev. A* **84**, 011803 (2011).
- [47] V. Loo, L. Lanco, A. Lemaître, I. Sagnes, O. Krebs, P. Voisin, and P. Senellart, *Appl. Phys. Lett.* **97**, 241110 (2010).
- [48] P. Borri, W. Langbein, S. Schneider, U. Woggon, R. L. Sellin, D. Ouyang, and D. Bimberg, *Phys. Rev. Lett.* **87**, 157401 (2001).
- [49] D. Birkedal, K. Leosson, and J. M. Hvam, *Phys. Rev. Lett.* **87**, 227401 (2001).
- [50] W. Langbein, P. Borri, U. Woggon, V. Stavarache, D. Reuter, and A. D. Wieck, *Phys. Rev. B* **70**, 033301 (2004).
- [51] D. Heiss, S. Schaeck, H. Huebl, M. Bichler, G. Abstreiter, J. J. Finley, D. V. Bulaev, and D. Loss, *Phys. Rev. B* **76**, 241306 (2007).
- [52] B. D. Gerardot, D. Brunner, P. A. Dalgarno, P. Öhberg, S. Seidl, M. Kroner, K. Karrai, N. G. Stoltz, P. M. Petroff, and R. J. Warburton, *Nature (London)* **451**, 441 (2008).
- [53] D. Brunner, B. D. Gerardot, P. A. Dalgarno, G. Wüst, K. Karrai, N. G. Stoltz, P. M. Petroff, and R. J. Warburton, *Science* **325**, 70 (2009).
- [54] G. Bester, S. Nair, and A. Zunger, *Phys. Rev. B* **67**, 161306 (2003).